Epidemiological Modeling of SARS-CoV-2 Spread with Viral Inactivation Measures

Charles Xu

VIDER team

Abstract

In response to the SARS-CoV-2 pandemic, the direct inactivation of airborne viruses has been explored as a means of reducing viral transmission and curtailing the further spread of the pandemic. While the development of inactivation technology progresses, the effects inactivation may have on the spread of the pandemic and what rates of inactivation are needed to make a significant impact on the spread of the virus are unknown. A deterministic compartmental model was created to simulate the spread of the virus under various inactivation schemes. Increasing standalone the coverage of inactivation technology and the rate of inactivation all contribute to greater reductions in deaths and hospitalizations. The pandemic can be stopped with 60-70% coverage at already established rates of inactivation. With sub 5 minute inactivation, stopping the pandemic can occur with 50-60% coverage. Although coverage of this scale may be difficult to achieve, inactivation technology can halt upwards of 90% of viral transmission in specific locations, making it particularly useful for keeping essential operations running.

1 Introduction

Since the outbreak of the Severe Acute Respiratory Syndrome Coronavirus 2 (SARS-CoV-2) in December 2019, non-pharmaceutical interventions (NPIs) have been widely employed to mitigate the spread of the virus [23]. Containment strategies employing NPIs such as travel bans and restrictions [5], contact reductions, social distancing, masking, early case identification, and isolation have all been applied with varying degrees of success [13]. The direct inactivation of airborne viruses to limit transmission is a promising NPI and unlike other NPIs, carries the additional benefit of not relying upon widespread social adherence.

The inactivation of viruses through resonant absorption of ultrasound energy has been the focus of recent studies, with theoretical work [1, 28, 7] being accompanied by the successful inactivation of influenza A virus [31]. Other methods utilizing chemical inactivation, UV radiation, pulsed lasers[27], non-thermal plasma reactors [30] and microwave thermal heating have all also been able to successfully inactivate a range of airborne viruses including coronaviruses [4]. Although it has not been performed yet, mathematical modeling of inactivation technology can work in tandem with the advancements in inactivation technology to determine how inactivation technology may affect the pandemic and guide its development and deployment.

Mathematical modeling of viral pathogens is frequently accomplished using compartmental modeling frameworks. A basic Susceptible-Infected-Recovered (SIR) model utilizes a nonlinear systems of differential equations that distributes the population into Susceptible, Infected and Recovered compartments. All individuals are assumed to be susceptible to the disease at the beginning of an outbreak because they have no acquired immunity. Over time, susceptible individuals become infected and eventually recover, with the rate of infection being dependent upon the number of infected and susceptible individuals. Upon recovery, individuals are assumed

to acquire immunity to the disease and are thus no longer susceptible to the disease [20]. The SIR model framework is quite flexible, and with proper modifications, can be applied to a wide array of diseases [20].

Basic SIR modeling and its derivatives have been used to model the spread and impacts of the coronavirus in various regions [25, 26, 3, 2], and have been used to analyze the effects of various intervention strategies such as interaction substitution [29] masking [8], social distancing[17] and travel bans [21] to name a few. This study is the first that models the effects of inactivation technology at the population level by using compartmental modeling.

2 Methods

2.1 Baseline model

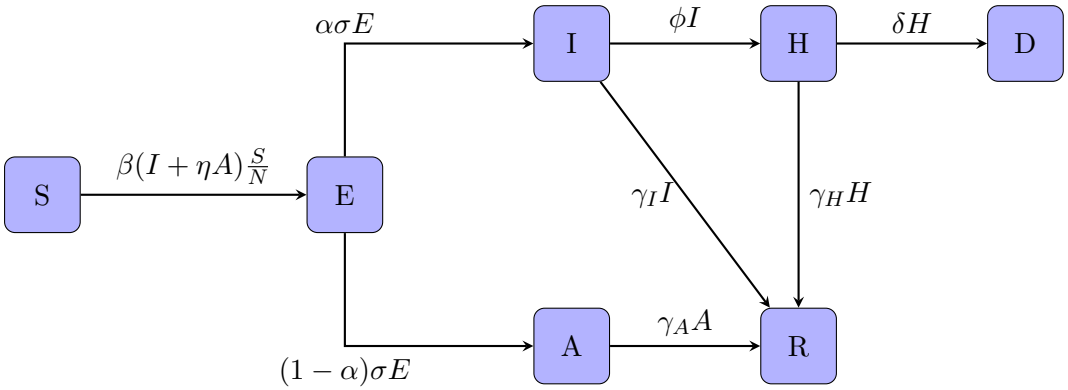

Figure 1: Flowchart summary of baseline Susceptible-Exposed-Infectious symptomatic-Asymptomatic infectious-Hospitalized-Dead (SEIAHRD) model of SARS-CoV-2 transmission. Parameters used in the model are given in Table 1.

A standard SIR model framework was expanded to better model the dynamics of coronavirus spread. The virus has an incubation time [14], asymptomatic infectious patients [11], and a significant hospitalized population that are not accounted for in a basic SIR framework. Thus the model accounts for susceptible, exposed, symptomatic infections, asymptomatic infectious, hospitalized, and recovered individuals, with the compartments denoted by S, E, I, A, H, and R respectively. An additional compartment D is used to keep track of deaths as shown in Figure 1. An intuition for the model is as follows: individuals become exposed to the virus depending on the infectious contact rate, number of infected individuals (symptomatic and asymptomatic), and the number of susceptible individuals. After being exposed, a certain proportion will become infected either symptomatically or asymptomatically. After becoming infected with symptoms, some individuals will become hospitalized. Hospitalized, symptomatic, and asymptomatic individuals recover at differing rates, and a fraction of hospitalized individuals will die.

The static parameters specific to SARS-CoV-2 needed for the model have been gathered from publications around the start of the outbreak and are summarized in Table 1. The baseline model can be implemented with 7 non-linear differential equations – one for each compartment.

2.2 Inactivation power

Coronavirus transmission occurs via direct contact, respiratory droplets and airborne transmission [16, 18], with viral transmission from direct contact likely to decrease in response to social protocol and preventative measures. The Independent Action Hypothesis (IAH) of viral transmission states that each virion has an equal, nonzero probability of causing an infection. Based

Table 1: Baseline static parameters chosen for this study based on reported values and clinical studies as documented in literature. The values of these parameters varies by region and over time.

Parameter	Definition	Value
β	Baseline infectious contact rate [8]	.5
σ	Transition rate from exposed to infectious class [14]	.196
α	Fraction of cases that are symptomatic [12]	.2
η	Relative infectiousness of asymptomatic carriers [15]	.5
ϕ	Rate at which symptomatic individuals are hospitalized [9]	.015
δ	SAR-CoV-2 case fatality rate (CFR) [9]	.015
$\gamma_I, \gamma_A, \gamma_H$	Recovery rates of infections, asymptomatic and hospitalized cases [8]	$\frac{1}{7}, \frac{1}{7}, \frac{1}{14}$

off the IAH, this model supposes that the probability of infection is proportional to number of airborne viral particles. Airborne particles will naturally decrease over time as they fall to the ground [24]. This natural decrease follows an exponential decay model. The implementation of inactivation technology will result in some particles no longer being viable as infectious candidates in accordance with the rate of inactivation. Due to the absence of experimental data to model the exponential rate of inactivation, a conservative assumption of inactivation occurring at a linear rate was made for the model.

The given assumptions allow for the additional incorporation of a new parameter ϵ that describes the relative efficiency at reducing viral transmission according to the following equations:

$$A = \int_0^{\infty} A_0 e^{kt} dt \tag{1}$$

$$A(t_I) = \int_0^{\frac{-1}{k} W(-k * t_I)} (A_0 e^{kt} - \frac{A_0 x}{t_I}) dt \tag{2}$$

$$\epsilon = \frac{A - A(t_I)}{A} \tag{3}$$

Where A is the total exposure to viral particles, A_0 is the initial count of particles in air, k is the continuous growth rate, t is time in minutes, $A(t_I)$ is the adjusted exposure to viral particles with inactivation, t_I is the time to completely eliminate the virus and W is the Lambert W function. A_0 was set to 6.8836 and k was set to -0.061 based on findings from Stadnytskyi *et al.* 2020.

2.3 Final model

The baseline model described in section 2.1 was expanded to account for inactivation. Because inactivation technology can either provide protection or no protection to an individual at a given time, a final partition dividing each compartment in the baseline model into protected and unprotected compartments is needed. To be considered protected at any given time, an individual must be exposed to viral inactivation technology and experience inactivation at the specified rate. After the division, 14 differential equations are needed to represent the population. The logic for the the final model is the same as the baseline model, but now the ϵ factor reduces transmission in protected interactions, and each compartment in the baseline model has two corresponding compartments that need to be accounted for at each step. The model is built off work done by Eikenberry *et al.* 2020 to model the impacts of masking on viral spread, with the key difference that inactivation technology does not directly help individuals that are not exposed to it.

$$\frac{dS_U}{dt} = -\beta(I_U + \eta A_U)\frac{S_U}{N} - \beta(I_P + \eta A_P)\frac{S_U}{N} \tag{4}$$
$$\frac{dE_U}{dt} = \beta(I_U + \eta A_U)\frac{S_U}{N} + \beta(I_P + \eta A_P)\frac{S_U}{N} - \sigma E_U \tag{5}$$
$$\frac{dI_U}{dt} = \alpha\sigma E_U - \phi I_U - \gamma_I I_U \tag{6}$$
$$\frac{dA_U}{dt} = (1-\alpha)\sigma E_U - \gamma_A A_U \tag{7}$$
$$\frac{dH_U}{dt} = \phi I_U - \delta H_U - \gamma_H H_U \tag{8}$$
$$\frac{dR_U}{dt} = \gamma_I I_U + \gamma_A A_U + \gamma_H H_U \tag{9}$$
$$\frac{dD_U}{dt} = \delta H_U \tag{10}$$
$$\frac{dS_P}{dt} = -\beta(1-\epsilon)(I_U + \eta A_U)\frac{S_P}{N} - \beta(1-\epsilon)(I_P + \eta A_P)\frac{S_P}{N} \tag{11}$$
$$\frac{dE_P}{dt} = \beta(1-\epsilon)(I_U + \eta A_U)\frac{S_P}{N} + \beta(1-\epsilon)(I_P + \eta A_P)\frac{S_P}{N} - \sigma E_P \tag{12}$$
$$\frac{dI_P}{dt} = \alpha\sigma E - \phi I - \gamma_I I \tag{13}$$
$$\frac{dA_P}{dt} = (1-\alpha)\sigma E - \gamma_A A \tag{14}$$
$$\frac{dH_P}{dt} = \phi I - \delta H - \gamma_H H \tag{15}$$
$$\frac{dR_P}{dt} = \gamma_I I + \gamma_A A + \gamma_H H \tag{16}$$
$$\frac{dD_P}{dt} = \delta H \tag{17}$$

The subscript U denotes interactions that are unprotected and P represents interactions that are protected by viral inactivation technology.

$$N = S_U + E_U + I_U + A_U + H_U + R_U + D_U + S_P + E_P + I_P + A_P + H_P + R_P + D_P \tag{18}$$

The total population size (N) is the sum of all of the compartments in the model.

The differential equations are numerically solved using 4th and 5th order Runge-Kutta methods. The model was run for 500 simulated days with initial starting conditions of a population of 328.2 million, 50 exposed individuals, and 20 confirmed cases.

3 Results

3.1 Initial model results

The model was initiallly run to compare the effects of half protection with inactivation technology. An ϵ value corresponding to 15 minute inactivation time was used as a baseline [31]. At all ranges of coverage for protection of the population, as the infection spreads, the number of recovered individuals increases. As more individuals recover, the number of susceptible individuals decreases due to the build up in the population's acquired immunity. Towards the end of the simulation, herd immunity is achieved and the population converges to an equilibrium as seen in Figure 2. The number of susceptible individuals decreases monotonically while the number in recovered and dead compartments both increase monotonically. The number of infections and

hospitalizations peak around 250 days, and then decrease due to the recovered individuals that limit the further spread of the virus.

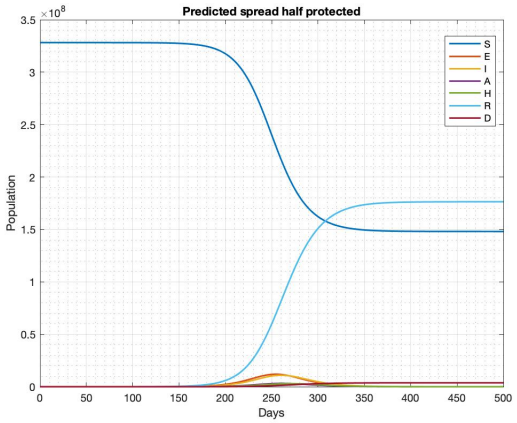

Figure 2: Simulated spread of SARS-CoV-2 through a model population. While this plot is for half protection, it is representative of most scenarios unless viral spread is significantly halted by inactivation technology.

A direct comparison of cumulative cases and deaths between 50% protection and no protection is able to further illustrate the effects of protection on populations. In response to half protection, there is a decrease in the total amount of cases and the spread of the virus is slowed (Figure 3a). The same trend is observed with deaths, where the total number is lower and the deaths are distributed over a longer period of time (Figure 3b). 5 different schemes are shown in Figure 3c, where an increase in percentage of protection is accompanied with a marked decrease in the peak hospitalization amount and the total number of hospitalizations. At 100% protection, the viral spread is halted and there is no noticeable increase in hospitalizations. The simulated hospital scenarios demonstrates the use of inactivation technology for "flattening the curve" and preventing the overflow of ICU bed capacity.

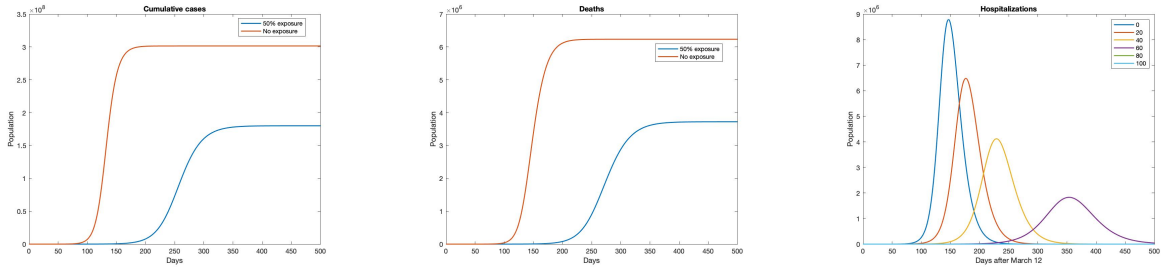

(a) (b) (c)

Figure 3: Increases in exposure to protection causes decreases in cumulative cases (3a), deaths (3b) and hospitalizations (3c). For cumulative cases and deaths, the scenarios of no protection and 50% protection are displayed, while for hospitalizations, 5 different levels of inactivation are displayed.

Total deaths and peak hospitalizations vary as a function of the percent protection and both decrease as the percent protection increases (Figure 4). Here, it is interesting to note that the response differs between deaths and peak hospitalizations. While peak hospitalizations decreases with a linear response for the majority of the domain, the response to total deaths is more nonlinear. Although the number of peak hospitalizations is linear for a significant portion of the domain, the number of total hospitalizations resembles total deaths.

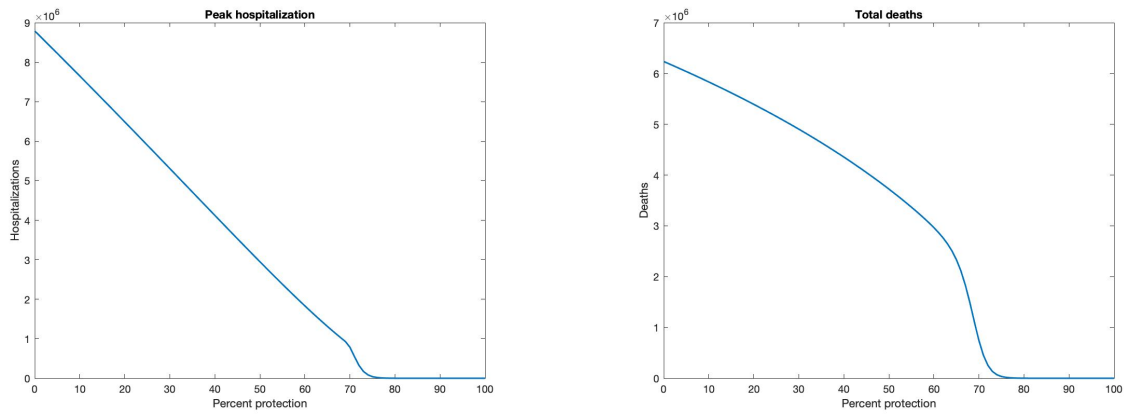

(a) (b)

Figure 4: Response of hospitalization (4a) and deaths (4b) to the percentage of individuals exposed to inactivation technology. Results with 15 minute inactivation.

3.2 Percent coverage and inactivation time

Within the model, inactivation technology functions by increasing the parameter ϵ. Epsilon values follow an exponential model. Therefore, greater marginal benefits should be observed as the inactivation time approaches zero (Figure 5).

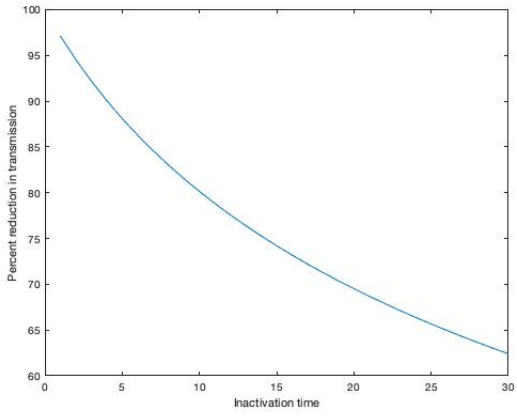

Figure 5: ϵ values are expressed as percent reductions in relative transmission.

Figure 6a demonstrates the results of a numerical experiment where inactivation time and percent exposure are varied. As inactivation time ranges from 1-25 minutes, the corresponding ϵ values range from 0.971 to 0.657. Percent reduction in deaths depends on both the percent protection and the time for inactivation. The heatmap demonstrates that inactivation technology can achieve total inactivation with a sufficient percent protection and a sufficiently fast inactivation time. There is a steep increase in percent reduction in deaths as the protection and inactivation time approach critical boundaries (Figure 6b). The relationship between inactivation time and percent coverage to achieve a 99.5% reduction in deaths can be approximated by the second order polynomial:

$$C = -0.0129T_I^2 + 1.4121T_I + 53.74 \tag{19}$$

where C is percent coverage and T_I is inactivation time.

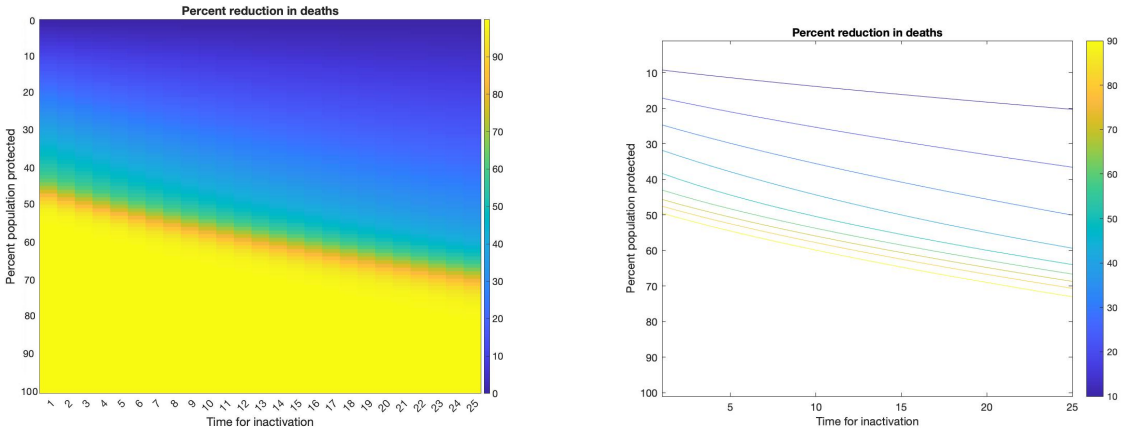

(a) (b)

Figure 6: Heatmap showing the relation between percent protection and time for inactivation. The simulation results are expressed with relative total mortality to show the relationship between a range of 0 to 100 for percent protection and 1 to 25 minutes for inactivation time. UVC inactivation occupies the slower range of inactivation at 25 minutes and microwave structure-resonant energy transfer as seen in Yang *et al.* 2015 is placed around 15 minutes. VIDER inactivation occurs in the sub 5 minute range. The corresponding contour plot is shown in 6b.

3.3 Linearity of response

The response from percent deaths is non-linear for both percent protection and inactivation time. For varying percent protection, the response has an initial period of linearity, but the effect in percent reduction in deaths increases rapidly after a certain percent protection. Inactivation time also follows a non-linear pattern, where the percent reduction in deaths accelerates as the inactivation time approaches zero (Figure 7a). The non-linearity in inactivation time can be simply explained by changes to ϵ as shown in Figure 5.

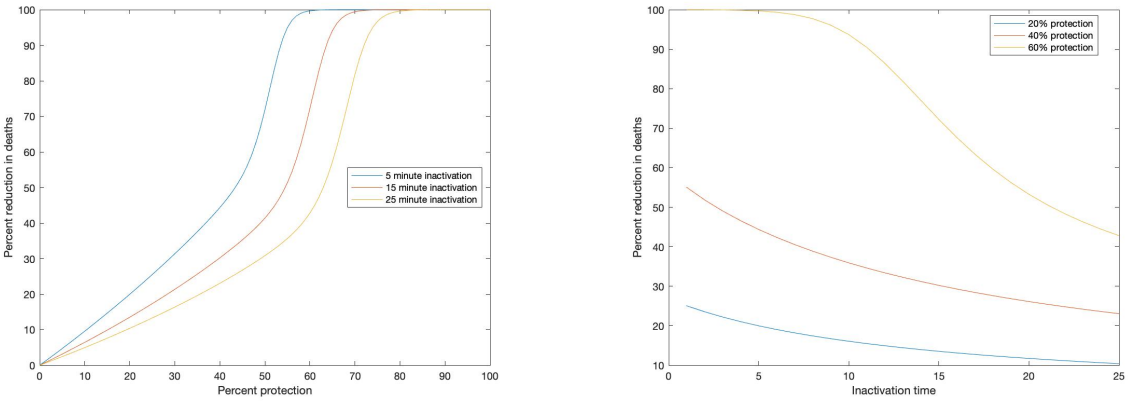

(a) (b)

Figure 7: Reaction in percent reduction in deaths to varying protection coverage (7a) and inactivation time (7b). In Figure 7a the three scenarios are based off of a 15 minute inactivation time.

4 Discussion

4.1 Efficacy and deployment

Inactivation technology has been rapidly developed to address the spread of SARS-CoV-2 and future pandemics. While experiments demonstrating the effect of the inactivation technology on samples of the virus have been performed, the epidemiological modeling of viral spread under inactivation methods done in this study contributes to the discussion of inactivation technology being effective at the population level. At all tested inactivation times, inactivation technology can serve as a standalone technology to slow or halt the pandemic. With 57% coverage, a 5 minute inactivation time can prevent 99.5% of deaths. At the population level, coverage is the driving factor for reducing spread. Improvements to inactivation rate has a comparatively limited capacity to induce population-level change.

Although inactivation technology can theoretically serve as a standalone intervention for halting pandemics, it is difficult to get the widespread coverage required to prevent the spread of the virus. Because the viral particles are directly affected, inactivation technology will directly lower the effective transmission rate of the virus. As effective transmission rate decreases to critical values, the response in reduction in deaths is highly non-linear. Therefore, inactivation technology works syngergistically with other NPIs. The deployment of inactivation technology must complement other public health control measures and NPIs rather than acting as a substitute. Maintaining the same preventative measures as key because inactivation technology may produce overconfidence among the public.

Much of inactivation technology's success is dependent upon gaining widespread coverage with inactivation technology, but this could be a complicated and costly endeavor. It is estimated that for influenza, 30% of transmission occurs within the household, 23% occurs in the general community, 26% occurs in schools and workplaces, and the remaining 21% occurs elsewhere outside of the household [10]. While data is not yet available for the coronavirus, distribution of inactivation technology to such varied sites of transmission poses a large challenge. SARS-CoV-2 spread is unevenly distributed amongst communities [6]; as a result estimating the population-level effects can become more nebulous. Development of inactivation technology in most affected regions is the most efficient way to have population-level impacts.

Attaining widespread coverage serves as a bottleneck in the population level effects of inactivation technology, but there is significant use for the local application of inactivation technology. As shown in Figure 5 it is possible for inactivation to have significant percent reductions in transmission as calculated by their ϵ values. Inactivation technology can contribute a $> 90\%$ reduction in baseline transmission. When used in tandem with other preventative methods, certain areas such as schools and hospitals can become safe for the general public. Because coverage can be complete when used in specific locations, the efficacy will be driven by the rate of inactivation. In these applications, sub 5 minute inactivation should be the desired goal so $> 90\%$ reductions in transmission can be achieved.

4.2 Model limitations

Only the final time required for full inactivation is reported in literature, so the assumption that the inactivation of virus occurs in a linear fashion had to be made for the model to run. It is likely that virus inactivation follows an exponential decay model, but owing to the lack of literature data on the progression of inactivation, there was no starting point to deviate from a linear model. It is recommended that future studies on inactivation technology report experimental data for the rates of inactivation to better assess the effects of the inactivation technology.

As noted in section 2.2, direct contact serves as an important means of transmission. As contact reduction and social distancing are implemented, it seems likely that transmission from direct contact should decrease. While not explicitly accounted for in the modeling parameters,

it is still unknown how inactivation technology affects airborne viruses and viruses on surfaces differently. More experimental data is needed before improvements can be made to this sort of model. Additionally, the complexity of the model can be increased to aid in the development of the inactivation technology. For example, models incorporating contact network structures and agent-based models could help to determine sites for the most efficient deployment of inactivation technology at a local level and allow for finer modeling of viral spread. Attempts and suggestions to improve the compartmental model are discussed in the appendices.

5 Conclusion

Numerical experimentation via the compartmental SEIAHRD model demonstrates that the effects of inactivation technology depends on inactivation time and coverage. While the pandemic may be stopped using only viral inactivation technology, this requires widespread coverage and efficient inactivation. Inactivation technology may be best suited for essential operations, where the reduction in viral transmission will be a function of the inactivation rate. The reduction of viral transmission accelerates with decreases in inactivation time, so improving the rate of inactivation even slightly can yield significant results.

Acknowledgements

I would like to thank my mentors Bryan Gamboa and Stacey Martens, the VIDER team, the Air Force Research Laboratory (ARFL), the Department of Defense, and the Center for Excellence in Education (CEE) for their support and guidance.

References

[1] M. Babincová, P. Sourivong, and P. Babinec. Resonant absorption of ultrasound energy as a method of HIV destruction. *Medical Hypotheses*, 55(5):450–451, 2000.

[2] Milan Batista. Estimation of the final size of the COVID-19 epidemic. *medRxiv*, (Nesteruk):1–11, 2020.

[3] David W Berger, Kyle F Herkenhoff, and Simon Mongey. An seir infectious disease model with testing and conditional quarantine. Technical report, National Bureau of Economic Research, 2020.

[4] Manuela Buonanno, David Welch, Igor Shuryak, and David J. Brenner. Far-UVC light efficiently and safely inactivates airborne human coronaviruses. *Research Square*, pages 1–21, 2020.

[5] Matteo Chinazzi, Jessica T Davis, Marco Ajelli, Corrado Gioannini, Maria Litvinova, Stefano Merler, Ana Pastore y Piontti, Kunpeng Mu, Luca Rossi, Kaiyuan Sun, et al. The effect of travel restrictions on the spread of the 2019 novel coronavirus (covid-19) outbreak. *Science*, 368(6489):395–400, 2020.

[6] Merlin Chowkwanyun and Adolph L Reed Jr. Racial health disparities and covid-19—caution and context. *New England Journal of Medicine*, 2020.

[7] Eric C Dykeman and Otto F Sankey. Low frequency mechanical modes of viral capsids: an atomistic approach. *Physical review letters*, 100(2):028101, 2008.

[8] Steffen E. Eikenberry, Marina Mancuso, Enahoro Iboi, Tin Phan, Keenan Eikenberry, Yang Kuang, Eric Kostelich, and Abba B. Gumel. To mask or not to mask: Modeling the potential

for face mask use by the general public to curtail the COVID-19 pandemic. *Infectious Disease Modelling*, 5:293–308, 2020.

[9] Neil Ferguson, Daniel Laydon, Gemma Nedjati Gilani, Natsuko Imai, Kylie Ainslie, Marc Baguelin, Sangeeta Bhatia, Adhiratha Boonyasiri, ZULMA Cucunuba Perez, Gina Cuomo-Dannenburg, et al. Report 9: Impact of non-pharmaceutical interventions (npis) to reduce covid19 mortality and healthcare demand. 2020.

[10] Neil M. Ferguson, Derek A.T. Cummings, Christophe Fraser, James C. Cajka, Philip C. Cooley, and Donald S. Burke. Strategies for mitigating an influenza pandemic. *Nature*, 442(7101):448–452, 2006.

[11] Nathan W Furukawa, John T Brooks, and Jeremy Sobel. Evidence supporting transmission of severe acute respiratory syndrome coronavirus 2 while presymptomatic or asymptomatic. *Emerging infectious diseases*, 26(7), 2020.

[12] Gwang-un Kim, Min-Jae Kim, Sang Hyun Ra, Jeongsoo Lee, Seongman Bae, Jiwon Jung, and Sung-Han Kim. Clinical characteristics of asymptomatic and symptomatic patients with mild covid-19. *Clinical Microbiology and Infection*, 2020.

[13] Shengjie Lai, Nick W Ruktanonchai, Liangcai Zhou, Olivia Prosper, Wei Luo, Jessica R Floyd, Amy Wesolowski, Mauricio Santillana, and Chi Zhang. outbreak in China. pages 1–29, 2020.

[14] Stephen A Lauer, Kyra H Grantz, Qifang Bi, Forrest K Jones, Qulu Zheng, Hannah R Meredith, Andrew S Azman, Nicholas G Reich, and Justin Lessler. The incubation period of coronavirus disease 2019 (covid-19) from publicly reported confirmed cases: estimation and application. *Annals of internal medicine*, 172(9):577–582, 2020.

[15] Ruiyun Li, Sen Pei, Bin Chen, Yimeng Song, Tao Zhang, Wan Yang, and Jeffrey Shaman. Substantial undocumented infection facilitates the rapid dissemination of novel coronavirus (sars-cov-2). *Science*, 368(6490):489–493, 2020.

[16] Lidia Morawska and Junji Cao. Airborne transmission of sars-cov-2: The world should face the reality. *Environment International*, page 105730, 2020.

[17] Samuel M Mwalili, Mark Kimathi, Viona Ojiambo, Duncan K Gathungu, and Rachel W Mbogo. SEIR model for COVID-19 dynamics incorporating the environment and social distancing. *Interventions*, 9:10, 2020.

[18] World Health Organization et al. Modes of transmission of virus causing covid-19: implications for ipc precaution recommendations: scientific brief, 27 march 2020. Technical report, World Health Organization, 2020.

[19] Liangrong Peng, Wuyue Yang, Dongyan Zhang, Changjing Zhuge, and Liu Hong. Epidemic analysis of covid-19 in china by dynamical modeling. *arXiv preprint arXiv:2002.06563*, 2020.

[20] Aaron Thomas Porter. A path-specific approach to SEIR modeling. 2012.

[21] Anca Radulescu and Kieran Cavanagh. Management strategies in a SEIR model of COVID 19 community spread. pages 1–13, 2020.

[22] Ruy Freitas Reis, Bárbara de Melo Quintela, Joventino de Oliveira Campos, Johnny Moreira Gomes, Bernardo Martins Rocha, Marcelo Lobosco, and Rodrigo Weber dos Santos. Characterization of the covid-19 pandemic and the impact of uncertainties, mitigation strategies, and underreporting of cases in south korea, italy, and brazil. *Chaos, Solitons & Fractals*, page 109888, 2020.

[23] Catrin Sohrabi, Zaid Alsafi, Niamh O'Neill, Mehdi Khan, Ahmed Kerwan, Ahmed Al-Jabir, Christos Iosifidis, and Riaz Agha. World Health Organization declares global emergency: A review of the 2019 novel coronavirus (COVID-19). *International Journal of Surgery*, 76(February):71–76, 2020.

[24] Valentyn Stadnytskyi, Christina E Bax, Adriaan Bax, and Philip Anfinrud. The airborne lifetime of small speech droplets and their potential importance in SARS-CoV-2 transmission. pages 3–5, 2020.

[25] Biao Tang, Nicola Luigi Bragazzi, Qian Li, Sanyi Tang, Yanni Xiao, and Jianhong Wu. An updated estimation of the risk of transmission of the novel coronavirus (2019-nCov). *Infectious Disease Modelling*, 5:248–255, 2020.

[26] Biao Tang, Xia Wang, Qian Li, Nicola Luigi Bragazzi, Sanyi Tang, Yanni Xiao, and Jianhong Wu. Estimation of the transmission risk of the 2019-ncov and its implication for public health interventions. *Journal of clinical medicine*, 9(2):462, 2020.

[27] Shaw Wei D. Tsen, David H. Kingsley, Christian Poweleit, Samuel Achilefu, Douglas S. Soroka, T. C. Wu, and Kong Thon Tsen. Studies of inactivation mechanism of non-enveloped icosahedral virus by a visible ultrashort pulsed laser. *Virology Journal*, 11(1):1–9, 2014.

[28] Nikolaos Uzunoglu. Theoretical analysis of the induction of forced resonance mechanical oscillations to virus particles by microwave irradiation: Prospects as an anti-virus modality. 2020.

[29] Joshua S. Weitz, Stephen J. Beckett, Ashley R. Coenen, David Demory, Marian Dominguez-Mirazo, Jonathan Dushoff, Chung Yin Leung, Guanlin Li, Andreea Măgălie, Sang Woo Park, Rogelio Rodriguez-Gonzalez, Shashwat Shivam, and Conan Y. Zhao. Modeling shield immunity to reduce COVID-19 epidemic spread. *Nature Medicine*, 26(6):849–854, 2020.

[30] T Xia, A Kleinheksel, EM Lee, Z Qiao, KR Wigginton, and HL Clack. Inactivation of airborne viruses using a packed bed non-thermal plasma reactor. *Journal of Physics D: Applied Physics*, 52(25):255201, 2019.

[31] Szu Chi Yang, Huan Chun Lin, Tzu Ming Liu, Jen Tang Lu, Wan Ting Hung, Yu Ru Huang, Yi Chun Tsai, Chuan Liang Kao, Shih Yuan Chen, and Chi Kuang Sun. Efficient Structure Resonance Energy Transfer from Microwaves to Confined Acoustic Vibrations in Viruses. *Scientific Reports*, 5(December):1–10, 2015.

6 Appendix

6.1 Time dependent fitting

The parameters for the deterministic compartmental model are likely to change over time as behavior changes in response to the pandemic. The infectious contact rate, recovery rate and death rate are all modeled as time dependent parameters and are adapted for the model in this study in accordance with past work [19, 25].

$$\beta(t) = \beta_{min} + (\beta_0 - \beta_{min})e^{(-r(t-t_0))} \tag{20}$$

$$\delta(t) = \delta_{min} + (\delta_0 - \delta min)e^{(-r(t-t_0))} \tag{21}$$

$$\gamma(t) = \gamma_{min} + (\gamma_0 - \gamma min)e^{(-r(t-t_0))} \tag{22}$$

The three recovery rates $(\gamma_I, \gamma_A, \gamma_H)$ were reduced to a single γ that applied to all categories for easier fitting. The fitting of these parameters was achieved by using 80,000 iterations of the Nelder-Meade direct search method to minimize the mean squared error function. Data of reported cases was obtained from a repository compiled by the New York Times.

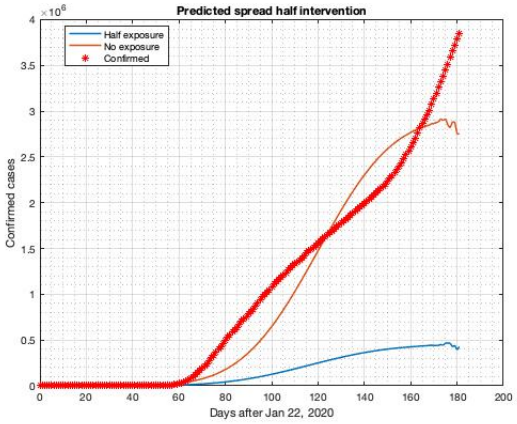

Figure 8: Cumulative confirmed cases for two modeled scenarios plotted against actual data.

As shown in Figure 8, the model fails to fit the data well over the entire course of the simulation. The time dependent parameters utilize an exponential decay model, but this isn't able to accurately describe the progression of the spread. An exponential decay model lacks the complexity to account for the rate of new cases increasing after 120 days. Further difficulties arise in using a data-driven approach due to limited testing and under reporting [22].

6.2 Machine learning of parameters

Rather than using a simple exponential decay model to adjust β values, it seemed appropriate to try and learn β values for the change to each individual day to get a finer model that could reflect changes in viral spread. β values were calculated by iterating through each day of the data and then calculating the value of β that would produce the closest fit to the data until that day. Machine learning was then used to fit a model to the calculated β. The model was trained using the Gaussian Process Regression Method with an exponential kernel, and the model was run using a time-dependent β as predicted by the trained model. While the model was able to very successfully fit to the calculated β values (Ref. Figure 9, the simulation's results differed greatly from the actual values. The model's issues stem from the daily β values that were calculated by the iterative method. Attempts to directly fit daily beta values by the Nelder-Mead direct search method were unsuccessful and still produced a poor fit to the data. However, if daily β values are able to be ascertained, utilizing a Gaussian Process Regression Method with an exponential kernel appears to be a viable method for precisely fitting parameters in data-driven models, and can generalize to future cases.

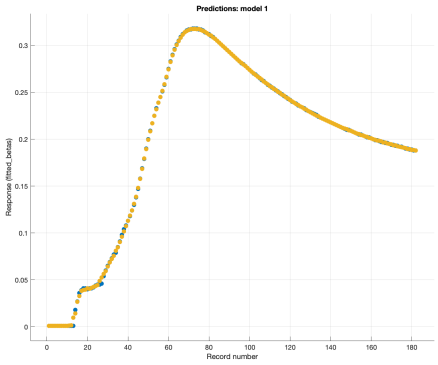

Figure 9: Actual values for β are in blue and model predictions are in yellow. There is very good overall agreement by using the Gaussian Process Regression Method.